CIRP Annals - Manufacturing Technology 71 (2022) 357–360

Contents lists available at ScienceDirect

CIRP Annals - Manufacturing Technology

journal homepage: https://www.editorialmanager.com/CIRP/default.aspx

Effectiveness of different closed-loop control strategies for deep drawing on single-acting 3D Servo Presses

Peter Groche (1)[a,*], Alexander Breunig[a], Kelin Chen[b], Dirk A. Molitor[a], Jinjin Ha[c], Brad L. Kinsey (2)[c], Yannis P. Korkolis[b]

[a] Institute for Production Engineering and Forming Machines, Technische Universität Darmstadt, Darmstadt, Germany
[b] Department of Integrated Systems Engineering, The Ohio State University, Columbus, OH 43210, USA
[c] Department of Mechanical Engineering, University of New Hampshire, Durham, NH 03824, USA

ARTICLE INFO

Article history:
Available online 14 May 2022

Keywords:
Deep drawing
Control
Servo press

ABSTRACT

Process specific actuators and sensors embedded in the tooling can enable closed-loop control of product properties in manufacturing processes to achieve desired final component characteristics. Alternatively, actuation conducted by the machine tool used and sensors positioned within the machine, i.e., outside of the tool, could increase robustness and reduce investment and installation costs for closed-loop control systems. This contribution presents and compares different closed-loop control strategies for deep drawing and demonstrates the advantages of machine based actuators and sensors in experiments and simulations.

1. Introduction

Deep drawing is an industrially highly relevant process for the mass production of hollow parts made of sheet metal. It is conventionally carried out on presses with a single drive and a die cushion, i.e., a single-acting press, or with two drives that are operated independently, i.e., a double-acting press. The occurrence of process limits, e.g., wrinkling and fracture, restricts the process window of deep drawing. Recently, two trends lead to narrower process windows: higher geometric complexity of the parts and lower ductility of high performance sheet metal, e.g., high strength aluminum alloys or steels.

Tighter process windows come along with a higher sensitivity to disturbances of equipment, material and process properties [1]. Allwood et al. considered sheet metal properties, e.g. coil-to-coil variation, as well as tribological conditions as the main disturbances in deep drawing processes [2]. These disturbances can lead to failures if the process is not adapted in an appropriate way.

Closed-loop control is a promising approach to cope with uncertainties arising from disturbances. It uses sensors to monitor the process, identifies the necessary process modification and uses actuators to adjust the process appropriately. Sensors used for closed-loop control of deep drawing mainly detect the material flow of the outer flange. The measured draw-in together with a model serves as a property sensor, which allows the prediction of the process adjustment. So far, actuators used to control deep drawing processes alter the material flow in the flange area by a second press drive for the blankholder, or actuators in the tools for draw bead or blankholder segments' adjustments. Drossel et al. proposed a force distribution measurement as an alternative sensor concept. They showed that critical deviations from the nominal course of the resulting total force lead to failures, which can be avoided by closed-loop control [3].

This brief summary of the state of the art in closed-loop control of deep drawing reveals important questions for future applications, including the necessary actuators. The paper at hand investigates the potential of single-acting presses without special tools, equipped with actuators for closed-loop control of deep drawing processes. The press used is a 3D Servo Press [4], which allows not only for the linear movement of the ram but also for its targeted tilting. So far, the effectiveness of different control strategies in deep drawing is not compared in the literature. This paper compares the outcome of different control strategies when coping with a disturbance. The study consists of numerical and experimental investigations. In order to draw sound conclusions from the observed actuation after a disturbance, a thorough validation of the numerical simulations of the closed-loop controlled processes is a significant part of this study.

2. Nominal case and its disturbance

The experiments were performed using a unique drawing tool with a gimbal-like blankholder (BH) system. A detailed description of the toolset can be found in [5]; here, only the basic features are discussed. Fig. 1 depicts the tool and the BH system. The BH is mounted on a carrier plate, which can tilt around one axis. This carrier plate itself is mounted on a secondary frame, which can tilt around an axis perpendicular to the first axis. This allows free tilting of the BH. The BH can be actuated through the tilting motion of the 3D Servo Press: that motion is transferred to a vertical displacement using cylindrical pins, which in turn compress the springs on the BH. By tilting the BH against the blank, the blankholder force (BHF) can be varied locally. The same drives move the punch in the vertical direction. Due to a ball coupling between punch and ram, the vertical translation of the

* Corresponding Author.
E-mail address: groche@ptu.tu-darmstadt.de (P. Groche).

https://doi.org/10.1016/j.cirp.2022.04.072
0007-8506/

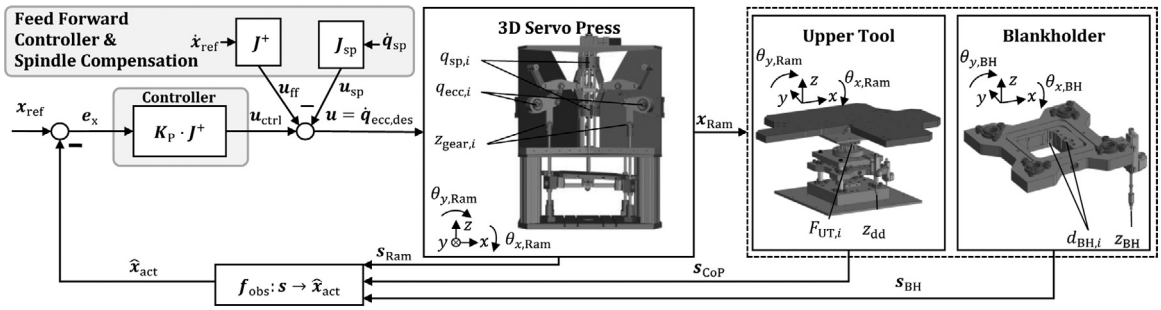

Figure 1. Generalized block diagram for experimentally investigated closed-loop control strategies (explanation of variables in Table 1).

punch and the tilting of the ram are independent of each other. Thus, separate closed-loop control of punch displacement and tilting of the BH is possible.

The material used for the experiments of this study is aluminum AA1100-O. It was received in the -H24 temper, laser-cut into circular blanks with a diameter of $D = 38$ mm and afterwards annealed at 343°C for 90 minutes using an industrial convection en (Nabertherm NA 15/65). After the heating period, the blanks were left to air-cool outside of the oven. The initial material thickness is 0.51 mm. The deep-drawing experiments were performed on a drawing tool with a punch diameter of $d_P = 20$ mm and a die diameter of $d_d = 21.3$ mm, resulting in a clearance of $c = 0.65$ mm. The drawing-ratio respectively is $\beta = D \cdot d_p^{-1} = 1.9$. The parts of the tool in contact with the blank are made from 1.2379 steel, surface hardened to a hardness of 62 HRC, as well as ground-finished to a surface roughness of $R_z = 2\ \mu$m. Before each experiment, a prelube (Multidraw PL 61 SE) was manually applied to both sides of the blank. An abundance of lubricant was used to ensure comparable tribological conditions throughout the tests. The BHF is generated by 8 springs (stiffness $k = 5.69$ N mm^{-1}), which are compressed by the downward movement of the ram, leading to a linearly increasing BHF throughout the drawing process. The springs are arranged in a circle of 60 mm diameter, spaced at 45° intervals to each other.

Using the aforementioned toolset, two experimental setups were implemented, i.e., one nominal case as a baseline and one perturbed case to test the performance of the control strategies. In the nominal case, blanks were drawn to a complete cup, i.e., with little flange remaining and a draw-depth of 12 mm. In the perturbed case, the setup was identical to the nominal case, but we loosened three springs in the first quadrant by 1 mm (see red marked springs in Fig. 2 and Fig. 4). Consequently, the resulting total force of the BH, referred to as the centre of pressure (CoP) in the following sections, moved away from the centre of the axisymmetric setup. Such misalignments of the springs represent typical conditions of wear or fatigue in real production. Furthermore, in the perturbed case, excessive wrinkling occurred, which prevented full drawing of the cup. Hence, this is a case where a successful process under nominal conditions, deviates to failure once it is perturbed. The objective of the control strategies will be to bring the system back to successful forming, i.e., no wrinkling.

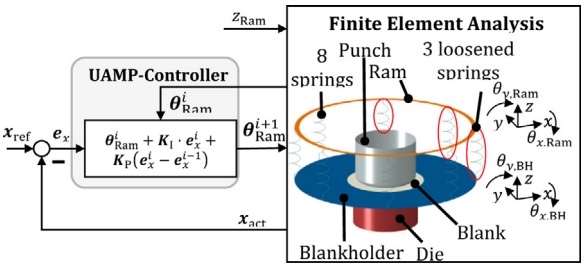

Figure 2. Diagram of the closed-loop controlled FE model. The controller was implemented using a User Amplitude subroutine (UAMP).

3. Closed-loop control system in reality

Three model-based closed-loop control strategies are compared. They differ fundamentally in the sensor signals s and controlled variables x used. All strategies are based on kinematic or kinematic-static control models f_{ctrl}, that establish functional relationships between the drives of the 3D Servo Press q and controlled variables x of the control loops. As presented in [6], special challenges such as non-linear transmission behaviour and kinematic singularities arise in the control of eccentric presses. These kinds of challenges are addressed with concepts from robotics [7].

The drives of the 3D Servo Press q can be divided into two spindle drives q_{sp} and three eccentric drives q_{ecc} that fulfil different tasks (see Fig. 1). While the spindles control the position of top and bottom dead centre, the eccentrics are used to manipulate the controlled variables of the different control strategies. The control models f_{ctrl}, establish a functional relationship between the press drives and the model-based estimated controlled variables, $\hat{x}$, and are based on kinematic or kinematic-static models. Eqn. 1-4

$$\hat{x} = f_{ctrl}(q) \tag{1}$$

A partial derivation of the model functions with respect to the eccentric drives leads to a quadratic and thus invertible Jacobian $J(q) \in \mathbb{R}^{3x3}$, which can be used in the controller to compensate for the non-linearity in the transfer behaviour of the press.

$$\dot{\hat{x}} = \frac{\mathrm{d}f_{ctrl}(q)}{\mathrm{d}t} = \frac{\mathrm{d}f_{ctrl}(q)}{\mathrm{d}q_{ecc}} \cdot \frac{\mathrm{d}q_{ecc}}{\mathrm{d}t} = J(q) \cdot \dot{q}_{ecc} \tag{2}$$

In order to guarantee singularity-robust control even at the dead centres of the machine, the Damped Least Square Inverse of the Jacobian as further described in [8]:

$$J^{+} = \left(J^{T}J + \lambda I\right)^{-1} \cdot J^{T} \tag{3}$$

is used for control. Knowing the control deviation e_x, which results from the desired reference variable x_{ref} and the observed variable $\hat{x}_{act}$, and using a P-controller with a diagonal gain matrix K_p, the manipulated variables for the eccentric drives $u = \dot{q}_{ecc,des}$ can be calculated. As shown in [6], a velocity control is superior compared to a position or torque control and a P-controller already eliminates control deviations completely. A feed forward controller calculates the eccentric velocities u_{ff} based on the desired velocity trajectory of the controlled variables $\dot{x}_{ref}$. The influence of the spindle velocities $\dot{q}_{sp}$ on the controlled variable is compensated by transforming the spindle velocities to eccentric velocities u_{sp} via a spindle Jacobian J_{sp}. This results in the manipulated variables for the eccentric drives:

$$u = \dot{q}_{ecc,des} = u_{ctrl} + u_{ff} - u_{sp}. \tag{4}$$

In order to implement the different control strategies, it is necessary to integrate various sensors that allow real-time calculation of the controlled variables with the aid of observer models. An overview of the sensors s, associated observer models f_{obs}, control models f_{ctrl} and controlled variables x for all investigated control strategies can be found in Table 1. The ram control aims at keeping the ram horizontal, without feedback from the process, while the CoP control tries to keep the location of the resulting BH force constant. The BH-control attempts to keep the BH parallel to the die. The positions of the sensors are revealed in the blocks of the block diagram in Fig. 1. While the ram pose is calculated from three position sensors $z_{gear,i}$ in the kinematic linkage of the 3D Servo Press, the calculation of the BH pose requires a much more sensitive measuring chain, which is realized via the two eddy current sensors (Micro-Epsilon eddyNCDT

Table 1
Used control strategies and related control models, sensors, observer models and controlled variables.

Control Type	Control model f_{ctrl}	Sensors s	Observer model f_{obs}	Controlled variables x
Ram control	Kinematic model $f_{ctrl,Ram}: q \rightarrow \dot{x}_{Ram}$	Three position sensors in the machine gear and linear resistive transducer $s_{Ram} = [\, z_{gear,1} \quad z_{gear,2} \quad z_{gear,3} \quad z_{dd} \,]^T$	Kinematic model $f_{obs,Ram}: s_{Ram} \rightarrow \hat{x}_{Ram}$	Two tilt angles of the ram and drawing depth $x_{Ram} = [\, \theta_{x,Ram} \quad \theta_{y,Ram} \quad z_{dd} \,]^T$
CoP control	Kinematic-static model $f_{ctrl,CoP}: q \rightarrow \dot{x}_{CoP}$	Three piezoelectric force sensors (upper tool) and linear resistive transducer $s_{CoP} = [\, F_{UT,1} \quad F_{UT,2} \quad F_{UT,3} \quad z_{dd} \,]^T$	Static model $f_{obs,CoP}: s_{CoP} \rightarrow \hat{x}_{CoP}$	X- and Y-coordinates of the CoP and drawing depth $x_{CoP} = [\, x_{CoP} \quad y_{CoP} \quad z_{dd} \,]^T$
BH control	Kinematic-static model $f_{ctrl,BH}: q \rightarrow \dot{x}_{BH}$	Two eddy current sensors and two linear resistive transducer $s_{BH} = [\, d_{BH,1} \quad d_{BH,2} \quad z_{BH} \quad z_{dd} \,]^T$	Kinematic-static model $f_{obs,BH}: s_{BH} \rightarrow \hat{x}_{BH}$	Two tilt angles of the blankholder and drawing depth $x_{BH} = [\, \theta_{x,BH} \quad \theta_{y,BH} \quad z_{dd} \,]^T$

3300) integrated in the BH. These measure two distances $d_{BH,i}$ between the BH and the die. The linear resistive transducer (Burster 8713-50) attached to the BH measures the vertical displacement of the BH center z_{BH}, during the process. Another transducer (Burster 8713-50) attached to the punch measures the drawing depth z_{dd}, which is controlled for all control strategies. The control of the CoP is based on the three force sensors (Kistler 9021A) in the upper tool $F_{UT,i}$, so that the CoP $[\, x_{CoP} \quad y_{CoP} \,]^T$ can be localized and controlled in the sheet plane. The control strategies presented are implemented on the programmable logic controller of the 3D Servo Press and are being called up with a sampling rate of 100 Hz. Since the control strategies only work when the sensors output meaningful values, the control strategies are activated at a drawing depth of 1 mm.

4. Closed-loop control deep drawing simulations

Closed-loop control strategies have been used in the simulations of deep-drawing processes, e.g., to control BHF to ensure optimal forming conditions [9]. Following a similar spirit, here we develop a finite element (FE) model in ABAQUS/Standard 2019 that enables closed-loop control of the ram tilting angles θ_{Ram}, BH tilting angles θ_{BH} or the reaction moments on the ram m_{Ram}. A schematic of the FE model is shown in Fig. 2. To be consistent with the experimental setup, the three "loosened" springs in the first quadrant were modeled as nonlinear springs with zero stiffness in the initial 1 mm compression and the nominal stiffness ($k = 5.69$ N mm^{-1}) afterwards. The full size blank was meshed using shell (S4R) elements and modeled with the Yld2000-2d yield function. Details about the material property characterization and friction coefficient identification can be found in [10, 11].

Specifically, for the CoP control case, two sensors were adopted to monitor the parameter x_{act}, which are reaction moments acting on the ram, $[\, m_{x,Ram} \quad m_{y,Ram} \,]^T$, at the beginning of each increment. The ram tilting angles about the x and y axes for each increment were prescribed using a PI controller as shown in Fig. 2. For the BH control case, two sensors were used to monitor the parameter x_{act} , which are the BH tilting angles, $[\, \theta_{x,BH} \quad \theta_{y,BH} \,]^T$. The ram tilting angles were prescribed using another set of PI control gains (gains: $K_P = -0.5$; $K_I = -5$). With the UAMP implemented, the ram tilting angles for each increment were prescribed to drive the CoP towards the origin for the CoP control case, or keep the BH tilting angle near zero for the BH control case. The controller was activated as the drawing process started, with about 600 loops used for the draw depth of 12 mm, consistent with the experiments.

5. Effectiveness of the control strategies

To validate the FE model, a comparison of the reaction moments and drawn cups at the draw depth of 12 mm from experiments and simulations for each closed-loop control strategy is presented in Fig. 3. The left column of cup snapshots is from the top-down view and the right column is from the isometric view of the same cup. Using ram control, considerable wrinkling occurs in the first (or top-right) quadrant, where the springs are loosened, and in the second (counter clock-wise) and fourth quadrants, too. This is well captured in the simulations, where the superimposed contour denotes the thickness distribution. It is also observed that the draw-in of the diagonal directions is more significant in the rolling direction (RD) and the transverse direction (TD), due to material anisotropy. The draw-in of the locally wrinkled region is even more significant because wrinkling reduces the circumference of the outer flange.

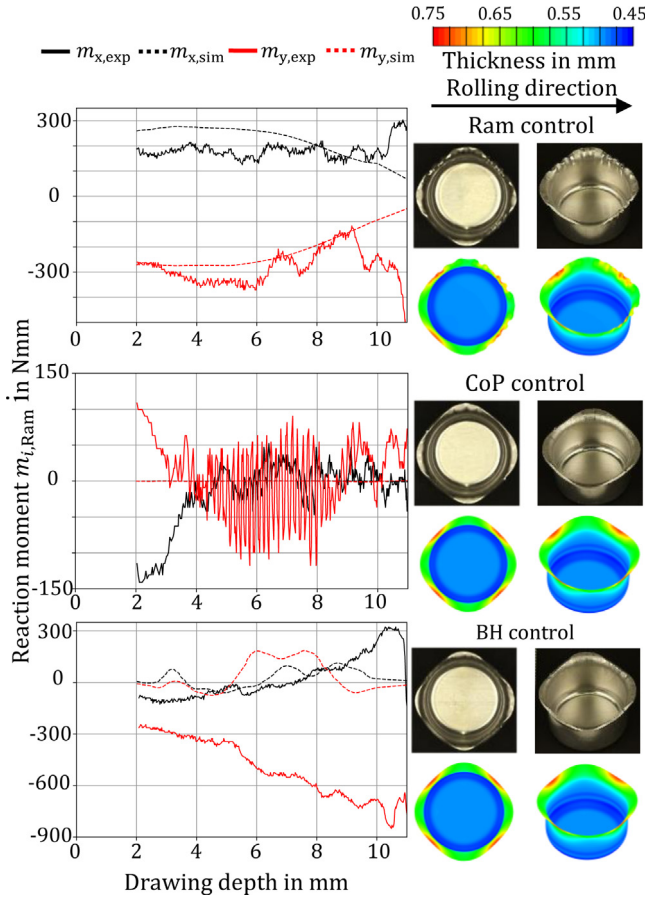

Figure 3. Comparison of the ram reaction moments (left) and cups from experiments and simulations using different control strategies (right).

The evolution trend of the measured and simulated reaction moments about both axes agrees well throughout the drawing process, with more pronounced deviations when the flange is almost completely drawn into the die at about 10 mm of drawing depth. The CoP control leads to completely wrinkle-free parts both, in the simulations and all experiments, which can be attributed to a significant reduction of the reaction moments in comparison to the ram control case. While almost zero reaction moments are calculated in the simulation, the measured ones oscillate with an amplitude of about 75 Nmm around the mean value of about 0 Nmm. The differences could be caused by effects not captured in the FEA (e.g. slight jamming of/friction in vertical pins). The BH control also leads to wrinkle-free cups from both the experiments and simulations. The evolution trend of the simulated and measured reaction moments around the x-axis agrees well. However, the moments about the y-axis deviate strongly from each other. This is because the BH is found to rotate in the negative x-axis direction, while in the simulations it rotates in the positive x-axis direction, which will be explained below.

To further validate the FE model, a comparison of the evolution of three key parameters from experiments and simulations is presented in Fig. 4. Fig. 4 (a,c,e) are the evolution of ram tilting angles, CoP and BH tilting angles from experiments, respectively, and Fig.4 (b,d,f) are the corresponding numerical results. Each figure includes the results from ram control (black line), CoP control (red line) and BH control (blue line). The corresponding images of the ram and BH at the corners of Fig. 4 show in which direction the respective components tilt in the experiments and simulations with the three loosened springs displayed in red. For the ram tilting angle in Figs. 4a and 4b, the ram control case gives zero angle for both the experiments and simulations because this is being prescribed. The CoP control case leads to a ram rotation about the 135° axis (right-hand rule), tilting towards the 45° direction for both experiments and simulations. This can be understood as each loosened spring in the first quadrant provides smaller force than the tightened spring, and the ram must tilt towards the first quadrant to compress those springs even more so that the eight spring forces are balanced. The ram tilting angle does not show pronounced evolution in both the experiments and simulations, indicating the CoP is effectively driven to the origin at the early drawing stages. For the BH control, the ram rotates about the 135° axis, tilting towards the 45° direction in the simulations to suppress local wrinkling in the first quadrant, as expected. However, in the experiments, the ram rotates about the 225° axis, tilting towards the 135° direction, possibly because a slight local wrinkling is detected in the second quadrant before the first quadrant. Despite that, the local wrinkling is suppressed with the BH control strategy in the experiments as well.

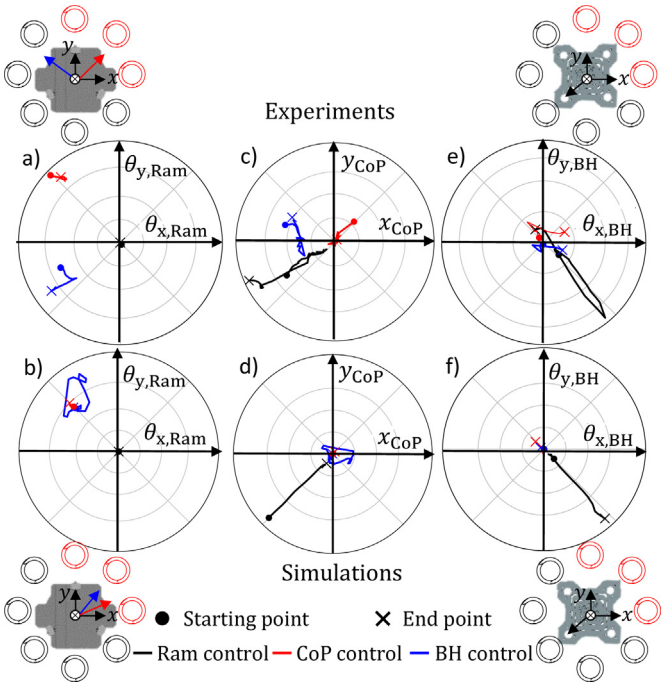

Figure 4. Comparison of the experimental a), c) and e) and simulated b), d), and f) curves of the controlled variables.

Because the tightened springs in the third quadrant provide larger force than the loosened ones in the first quadrant, the experimental and simulated CoP values are in the third quadrant causing the ram control case in Figs. 4c and 4d to also be in the third quadrant, far away from the origin. However, with the CoP control strategy, as the ram tilts towards the first quadrant (Figs. 4a and 4b), the eight spring forces are more balanced, and the CoP is thus quickly driven to the vicinity of the origin. This is similar in the simulated BH control case, because the ram tilts towards the first quadrant as it does in the simulated CoP control case (Fig. 4b). However, for the BH control in the experiments, the ram tilts towards the second quadrant. Therefore, the CoP tends to move from the initial second quadrant to the third one, eventually drifting around the x-axis. Despite that, this BH control strategy brings the CoP closer to the origin and effectively suppresses local wrinkling.Without CoP or BH controls, the local wrinkling in the first quadrant pushes up the BH. Therefore, the BH rotates about the 315° axis and tilts towards the 225° direction, as shown in Fig. 4e and 4f (black lines). With CoP or BH controls, the local wrinkling is successfully suppressed, as was shown in Fig. 3, and the BH remains almost flat. This is well captured by the nearly zero tilting angles in both experiments and simulations.Both the CoP and BH control strategies successfully suppress wrinkling around the flange, thus a cup can be drawn successfully, as shown in Fig. 3. The simulations reproduce the measured evolution of key variables quite well in Fig. 4, again confirming the efficiency of the FE model.

6. Conclusions and outlook

This paper shows for the first time how multi-dimensional control strategies can be realised on single-acting presses without additional actuated tools. Using the example of a deep drawing process, a closed-loop controlled numerical model is developed and three control strategies are tested, which are then examined experimentally on a 3D Servo Press. It is shown that simulation and experimental results are in reasonable agreement, leading to similar wrinkle formations on the parts, and that the selection of the closed-loop control strategy plays a key role in the part quality. Closed-loop controlled FE simulations are therefore a valuable tool to predict the operation of experimental closed-loop control strategies, even though they strongly depend on the robust acquisition of reliable measurements. Future work will address the control of more complex component geometries and explore data-driven approaches for trajectory planning.

Declaration of Competing Interest

The authors declare that they have no known competing financial interests or personal relationships that could have appeared to influence the work reported in this paper.

Acknowledgments

This research was supported by NSF award CMMI-1727490 and DFG award 386415239. This support is acknowledged with thanks.

References

[1] Doege E, Schmidt-Jürgensen R, Huinink S, Yun JW (2003) Development of an optical sensor for the measurement of the material flow in deep drawing processes. *CIRP Ann* 52(1):225–228.
[2] Allwood JM, Duncan SR, Cao J, Groche P, Hirt G, Kinsey B, Kuboki T, Liewald M, Sterzing A, Tekkaya AE (2016) Closed-loop control of product properties in metal forming. *CIRP Ann* 65(2):573–596.
[3] Drossel WG, Zorn W, Hamm L (2019) Modular system to measure and control the force distribution in deep drawing processes to ensure part quality and process reliability. *CIRP Ann* 68(1):309–312.
[4] Groche P, Scheitza M, Kraft M, Schmitt S (2010) Increased total flexibility by 3D Servo Presses. *CIRP Ann* 59(1):267–270.
[5] Breunig A, Hoppe F, Groche P. (2019) Localized Blank-Holder Pressure Control in Cup Drawing through Tilting of the Ram. NUMIFORM 2019: The 13th International Conference on Numerical Methods in Industrial Forming Processes: 583-586.
[6] Hoppe F, Pihan C, Groche P (2019) Closed-loop control of eccentric presses based on inverse kinematic models. *Procedia Manufacturing* 29:240–247.
[7] Oetomo D, Ang MH (2009) Singularity robust algorithm in serial manipulators. *Robotics and Computer-Integrated Manufacturing* 25(1):122–134.
[8] Hoppe F (2021) Modellbasierte Regelung der Stößelbewegung von Servopressen. Shaker Verlag Düren. *Berichte aus Produktion und Umformtechnik Bd* : 127.
[9] Sim HB, Boyce MC (1992) Finite element analyses of real-time stability control in sheet forming processes. *J. Eng. Mater. Technol.* 114(2):180–188.
[10] Ha J, Fones J, Kinsey BL, Korkolis YP (2020) Plasticity and formability of annealed, commercially pure aluminum: experiments and modeling. *Materials* 13 (19):4285.
[11] Chen K, Breunig A, Ha J, Kinsey B, Groche P, Korkolis YP (2022) Robustness of deep-drawing finite element simulations to process variations. *International Journal of Material Forming.*